Biomaterials 30 (2009) 1587–1595

Contents lists available at ScienceDirect

Biomaterials

journal homepage: www.elsevier.com/locate/biomaterials

Multi-layered culture of human skin fibroblasts and keratinocytes through three-dimensional freeform fabrication

Wonhye Lee [a,b], Jason Cushing Debasitis [a], Vivian Kim Lee [b], Jong-Hwan Lee [a], Krisztina Fischer [a], Karl Edminster [a], Je-Kyun Park [b], Seung-Schik Yoo [a,*]

[a] Department of Radiology, Brigham and Women's Hospital, Harvard Medical School, Boston, MA 02115, USA
[b] Department of Bio and Brain Engineering, KAIST, Daejeon 305-701, Republic of Korea

ARTICLE INFO

Article history:
Received 2 October 2008
Accepted 4 December 2008
Available online 23 December 2008

Keywords:
Tissue engineering
3D freeform fabrication
Skin tissue regeneration
Fibroblasts
Keratinocytes
Collagen hydrogel

ABSTRACT

We present a method to create multi-layered engineered tissue composites consisting of human skin fibroblasts and keratinocytes which mimic skin layers. Three-dimensional (3D) freeform fabrication (FF) technique, based on direct cell dispensing, was implemented using a robotic platform that prints collagen hydrogel precursor, fibroblasts and keratinocytes. A printed layer of cell-containing collagen was crosslinked by coating the layer with nebulized aqueous sodium bicarbonate. The process was repeated in layer-by-layer fashion on a planar tissue culture dish, resulting in two distinct cell layers of inner fibroblasts and outer keratinocytes. In order to demonstrate the ability to print and culture multi-layered cell–hydrogel composites on a non-planar surface for potential applications including skin wound repair, the technique was tested on a poly(dimethylsiloxane) (PDMS) mold with 3D surface contours as a target substrate. Highly viable proliferation of each cell layer was observed on both planar and non-planar surfaces. Our results suggest that organotypic skin tissue culture is feasible using on-demand cell printing technique with future potential application in creating skin grafts tailored for wound shape or artificial tissue assay for disease modeling and drug testing.

1. Introduction

Skin repair is important for the treatment of burns, lacerations and diabetic wounds. To restore the function of the skin after damage and to facilitate a wound-healing process, autologous grafts are commonly used to repair the skin while avoiding immune-rejection [1]. Extensive skin damage beyond the conventional graft extraction method requires rapid *in vitro* culture of biopsied skin cells to form a planar sheet of skin cells [2–4]. These sheets are transplanted back onto the wound site to prevent fluid loss and infection while promoting the skin repair process.

In order to address deeper skin damage involving dermal layers under the basal lamina, several techniques have been developed by combining biocompatible materials with key cellular components of skin grafts. For example, dermal cellular components such as fibroblasts (FB) are combined with a biomaterial matrix such as a silicone-based sheet [5] to stimulate cellular regeneration and vascularization at the wound site [6,7]. Autologous keratinocytes (KC) have also been integrated with a compatible xenotransplant of bovine collagen to assist the regeneration of both dermal and epidermal skin layers [8–10].

Stratified skin cellular structure is crucial for the regeneration of cell-to-cell and cell-to-extracellular matrix interactions necessary for normal skin function. Therefore, three-dimensional (3D) organotypic reconstruction of the multiple skin layers has been suggested for skin repair [8,11–13] and to model progresses of skin diseases or damages [14,15]. To artificially construct stratified layers of skin cells, dermal FB are seeded in a collagen scaffold below epidermal KC [16]. In cases where the organotypic skin culture is needed for the purpose of wound repair, 3D morphology of the skin construct, specifically tailored to the shape of patient's wound site, cannot be readily generated via conventional approaches.

Multi-layered biomimetic skin can be constructed through tissue engineering approaches, based on the soft-lithographic methods. In these methods, the spatial distribution of cells or cellular environment is patterned in layer-by-layer fashion [17–19]. Although the soft-lithographic approach can reliably generate the biological patterns in cell-level accuracy, it needs sophisticated production and co-alignment of individual lithographic masks for the production of a multi-layered cell structure [17–19]. A new technique, so-called on-demand 3D freeform fabrication (FF), has also emerged to construct tissues and organs in 3D, on-demand

* Corresponding author. Tel.: +1 617 525 3308; fax: +1 617 525 3330.
E-mail address: yoo@bwh.harvard.edu (S.-S. Yoo).

0142-9612/$ – see front matter © 2008 Elsevier Ltd. All rights reserved.
doi:10.1016/j.biomaterials.2008.12.009

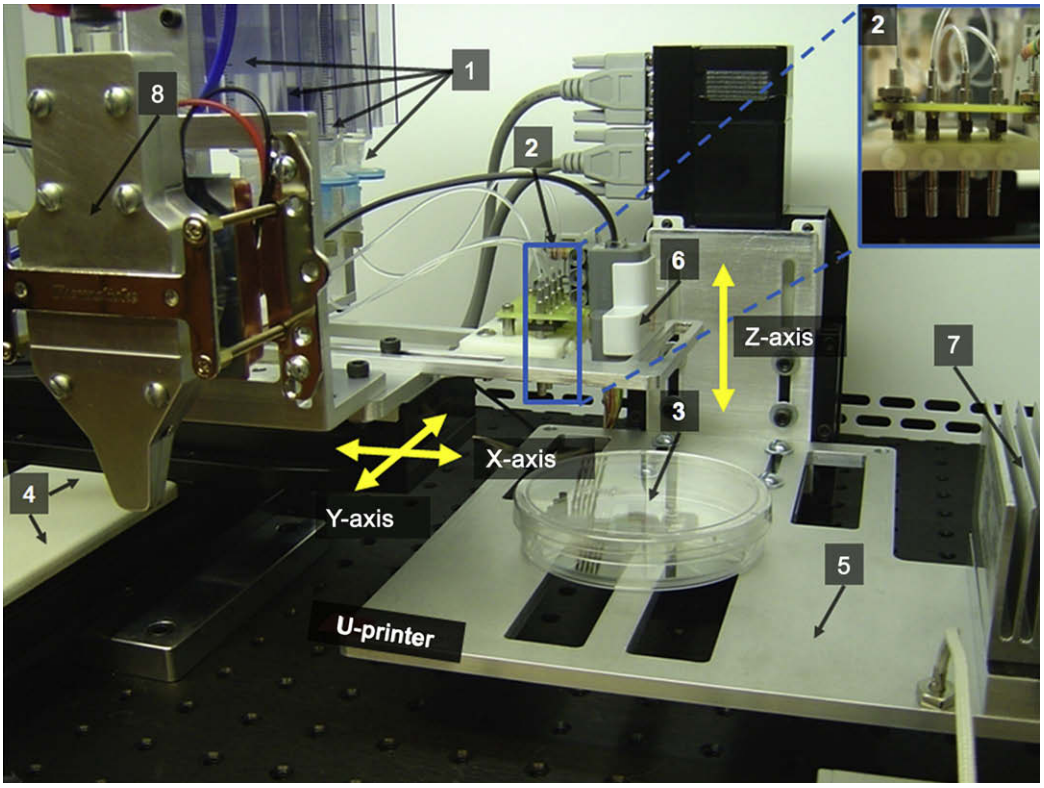

Fig. 1. Picture of the modular tissue printing platform shown with [1] 4 syringes as 'cartridges' to load cell suspensions and hydrogel precursors; [2] an array of 4-channel dispensers; [3] target substrate; [4] horizontal stage; [5] vertical stage; [6] range finder; [7] vertical stage heater/cooler; [8] optional independent heating/cooling unit for the dispenser. Inset: close-up view of the 4-channel micro-dispensers.

fashion [20,21]. The 3D FF technique allows for the construction of an artificial tissue, either autologous or non-autologous in nature, by printing cells and natural/synthetic biomaterials in strategic locations with the help of high-precision robot. The procedure involves printing a layer of hydrogel precursor in liquid state. The layer is crosslinked to form a hydrogel that provides structural integrity for the subsequent layer of printing, with cells and other extracellular matrices (ECM) embedded within. With the ultimate aim of replacing the function of the damaged tissue, the printed tissue construct can potentially be introduced to the target area after *in vitro* culture [22–25].

We report a novel method to construct stratified skin cell layers in 3D via robotic cell printing technique using an established *in vitro* human dermal/epidermal skin model [16]. The morphological information of the 3D tissue composite to be printed was converted layer-by-layer to two-dimensional (2D) planar information. The information was used to dictate printing motions for on-demand construction of the skin layers. Unlike the existing cell printing methods which require the planar target surface [26], we introduced a new 3D FF technique whereby layers of collagen precursor are printed via a non-contact dispenser and crosslinked by coating the precursor with a nebulized aqueous crosslinking agent (sodium bicarbonate). This process eliminated the needs of having separate planar containers for crosslinking agents/uncrosslinked polymers [26,27] and enabled direct, on-demand fabrication of the 3D tissue composites on non-planar surfaces. The feasibility of generating a computer-generated shape of skin replacement/graft was tested by printing the multi-layered skin cells onto the poly(dimethylsiloxane) (PDMS) mold that mimics a skin wound with a 3D surface contour. The stratified layers of printed FB and KC within the multi-layered collagen scaffold were confirmed through immunofluorescence confocal imaging.

2. Materials and methods

2.1. Overview of 3D bio-printer

The overall schematic of the printing hardware is shown in Fig. 1. The printer mainly consists of an array of four microvalves as dispensers and a three-axis Cartesian robotic stage. The dispensers, each with a pneumatically driven control mechanism, were mounted to the horizontal (x–y) robotic stage (Newmarksystems, CA), which controlled the timing and location of dispensing of printable materials including hydrogel precursors and cell suspensions. The target substrate was mounted to another robotic stage that moved along the vertical direction. The cell suspension in culture media and hydrogel precursors in aqueous form were placed in disposable plastic syringes and continuously fed to the dispensers under pneumatic pressure. The entire device was housed in a laminar flow hood (StreamLine, FL). A high-speed camera (Pixelink PL-A741; Ottawa, Canada) was used to measure the droplet size while two video cameras (UBV-49; Logitech, CA and MW200; MobiTechPlus Inc, Korea) monitored the stage movement as well as construction of the printed tissue. One of the dispenser units as well as the vertical stage was temperature controlled (operating temperature between 5 °C and 40 °C) by a solid-state thermoelectric device (TED; TE Technology, Traverse City, MI). Syringes and tubings used in this experiment were disposable and replaceable. All the hardware parts were designed in detachable modules for easy assembly and modification.

2.2. Software interface and hardware implementation

The MATLAB computing environment (Mathworks, Natick, MA) was used to generate the robot control codes dictating the dispensing spatial coordinates. Information on the target substrates, as input to the printer, was prepared from a slice-by-slice profile of the images representing the desired 3D structure. Alternatively, 3D computer-aided-design (CAD) files (SolidWorks, Concord, MA) or slice-by-slice 3D radiological images obtained from MRI or CT can be used as input files. For example, 2D information representing the sections of a 3D object can be obtained via virtually 'slicing' the volume through interpolation routines such as nearest neighbor or tri-linear methods [25,28]. The dispensing coordinates were then spatially sampled from the 2D sectional images. The distance between each dispensing points (printing resolution) along with the desired printing dimension was user-definable. The sampled printing coordinates are routed to the path planner algorithm (either through vector or coordinate-by-coordinate mode), which

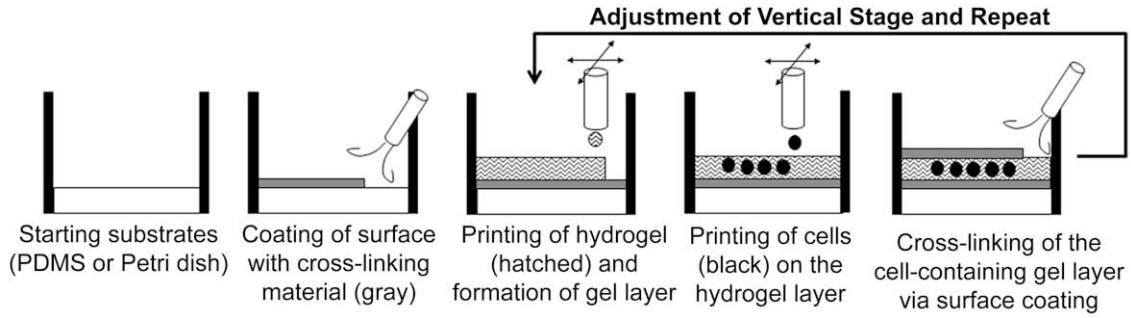

Fig. 2. The schematic of multi-layered composition of hydrogels and cells using administration of the nebulized crosslinking agent on the printed hydrogel precursors. Robotic stages were used to control the timing and location of the cell–hydrogel droplets.

prescribed the printing sequence. The path can be defined in either sequential line printing or boundary-printing followed by sequential filling. This process is similar to the printing routine for many types of commercial plotters. Spatial gradient of dispensing density as well as the clustering of dispensing sequence (to save printing time) can be implemented, with a 3D 'preview' function to help the user to plan or monitor the printing process. The generated control codes were sequentially executed by scripts generated by Active-X Toolkit (Galil Motion Control, Inc., Rocklin, CA) programmed in Visual Basic (Microsoft, Redmond, WA). The distance between the dispenser nozzle and target substrates was detected by an ultrasonic range finder (SRF04; Devantech, Norfolk, UK) mounted on the dispenser array, and maintained by adjusting the position of a vertical stage. The volume of droplet was changed independently across all four channels of dispensers by controlling the pneumatic pressure to the fluid paths or by controlling the gating duration of the valve-based dispenser. Other ECM materials or cytokines prepared as liquid can be dispensed and integrated into hydrogel during sequential dispensing.

2.3. Control of fluid dispensing

The general operating principle of the dispensing mechanism is explained as follows. Cell suspensions and uncrosslinked hydrogel precursors were placed in 5 or 10 mL disposable syringes. Each syringe was independently pressurized using an air tank while the pressure was controlled by a digital pressure regulator (ITV-2010; SMC, Japan). The fluidic pathway from the syringe, under the pneumatic pressure, was gated by a set of electromechanical microvalves (SMLD; Fritz Gyger AG, Thun-Gwatt, Switzerland, 150 μm nozzle diameters) using a standard TTL (Transistor-transistor logic) pulse (Electromechanica, East Freetown, MA). With the minimal open/close duration of 200 μs for the valve, the maximum duty cycle allowed at least 1000 Hz of dispensing. The advantage of using a pneumatically driven electromechanical valve is that various types of liquid materials with viscosities up to 200 Pa s can be dispensed by adjusting the pressure and valve gating time. Based on Bernoulli's principle of fluids, the droplet ejection speed was controlled by regulating syringe's pressure. The shock during surface impact is not much of a concern for cell viability since the printed cells were cushioned by the hydrogel bed at the ejection velocity used, which was typically less than 3 m/s, as measured by the installed high-speed camera. Unlike the potential pressure-related cell damage which could occur in ink-jet or piezoelectric element-driven dispensing, high cell viability was anticipated due to low operational pneumatic pressure, which was in the order of 1–3 psi.

2.4. Method of constructing multi-layered cell–hydrogel composites

To construct multi-layered cell–hydrogel composites, the dispensed liquid hydrogel precursors must be crosslinked to form a hydrogel layer before printing any subsequent layers. The dispensing of hydrogel precursors and crosslinking agents as liquid droplets onto the same location does not generate the desired printing pattern since two liquid drops, when placed in proximity, immediately form a single drop due to the surface tension. This tends to severely distort the intended morphology of the tissue constructs. The problem worsens when larger droplets exceeding 100 μm in diameter are used for patterning. Boland et al. [29] printed the crosslinker (containing calcium chloride) pattern onto the uncrosslinked hydrogel precursor (alginic acid), thus achieving patterns with a resolution of the droplet size, which was about 50 μm. More recently, Chang et al. [30] proposed the extrusion of viscous alginate hydrogel precursor as a continuous strand onto the bed of aqueous calcium chloride to form 3D micro-organ. These methods require a separate container to prepare a leveled surface of hydrogel or crosslinking materials, along with the risk of washing off the printed product during the crosslinking process.

To overcome this limitation, we adopted a new method to construct 3D hydrogel composites. As illustrated in Fig. 2, the substrate surface was coated with cross-linking agent. In this case, a sodium bicarbonate ($NaHCO_3$) solution (0.8 M concentration in distilled water), as pH-altering crosslinking agent, was nebulized via an ultrasonic transducer (SU-1051 W, Sunpentown, City of Industry, CA) operating at 2.5 MHz resonance frequency. The uncrosslinked collagen layer was then printed on the coated surface and crosslinked to form a gel due to the pH change. During this process, the generation of ultra-fine mists with droplets less than 2 μM in diameter was crucial to crosslink the dispensed collagen precursors without macroscopically distorting the printing morphology. The size of the dispensed hydrogel droplet, on the other hand, was in the order of 200–300 μm in diameter when it landed on the substrates. The droplets of cell suspension in culture media were then dispensed on the partially crosslinked hydrogel layer to be lodged inside. $NaHCO_3$ solution in nebulized form was then applied on the surface to crosslink the remainder of the collagen layer. The top surface coated with $NaHCO_3$ served as the crosslinking material for the next layer to be printed. The process was repeated to construct multiple layers of collagen and cells. Consequently, this technique can be applied on non-planar surfaces without the preparation of a separate container for crosslinking materials. The constructed multi-layered cell–hydrogel composites were incubated in 37 °C, 5% CO_2 for 20 min before the culture media was added.

2.5. Preparation and printing of collagen hydrogel precursor

Type I collagen (rat tail origin; BD Biosciences, MA) was used as hydrogel precursor for a scaffold material. The collagen precursor was diluted to 2.05 mg/mL with 1X Dulbecco's phosphate-buffered saline (DPBS) and kept on ice. The pH of the diluted collagen was approximately 4.5, which allowed the collagen remained uncrosslinked to be dispensable. After sterilizing the syringes and fluidic pathways (with 70% alcohol and distilled water; dried under the culture hood), the prepared collagen precursor solution was loaded into a syringe and subsequently printed to fill 10 by 10 mm square areas using the inter-dispensing distance (spatial resolution) of 600 μm. The droplets of collagen precursor were printed with a pressure of 2 psi and a valve opening time of 600 μs.

2.6. Cell culture and preparation for printing

Skin cell lines and cell culture reagents were purchased from ScienCell Laboratory (Carlsband, CA). Primary adult human dermal FB and primary adult human epidermal KC were purchased and cultured in standard condition of 37 °C, 5% CO_2, 2% fetal bovine serum and 1% FB growth supplements was added to FB media while 1% KC growth supplements were added to KC media. 1% penicillin–streptomycin was also added to both culture media. Culture media were changed every other day.

Both cell lines were subcultured when cells were grown to sufficient confluency. FB and KC were used for printing experiments at passage 6. The harvested cells were suspended in the required culture medium at a concentration of 1×10^6 cells/mL. While cell suspensions with lower concentrations ($<10^5$ cells/mL) did not promote the proliferation of printed cells in the collagen scaffold, those with concentrations higher than 3.0×10^6 cells/mL induced clogging problems in the dispenser with aggregated cell pellets. The syringes and fluidic pathways for cell printing were sterilized with 70% alcohol, flushed with endotoxin-free, distilled water and dried via HEPA filtered air. The cell suspensions were loaded in the syringes of the cell printer and gently vibrated during printing experiments to prevent cell aggregation. The droplets of cell suspension were printed with pressure of 1.2 psi with a valve opening time of 500 μs.

2.7. Testing of printing resolutions and patterning

Prior to 3D multi-layered cell–hydrogel printing, the growth tendencies of printed FB in the collagen hydrogel were monitored through bright-field microscopy. Six different printing resolutions (in terms of inter-dispensing distance) of 200, 300, 400, 500, 700 and 900 μm were examined for printing FB in the collagen hydrogel. The FB suspension (concentration of 1×10^6 cells/mL) was printed in the upper layer of two collagen layers and the growth tendency was monitored on culture days 1 and 8. With printing resolution of 300 μm, the FB reached cell confluency within 10 days after printing (see 3. Results); therefore, the printing

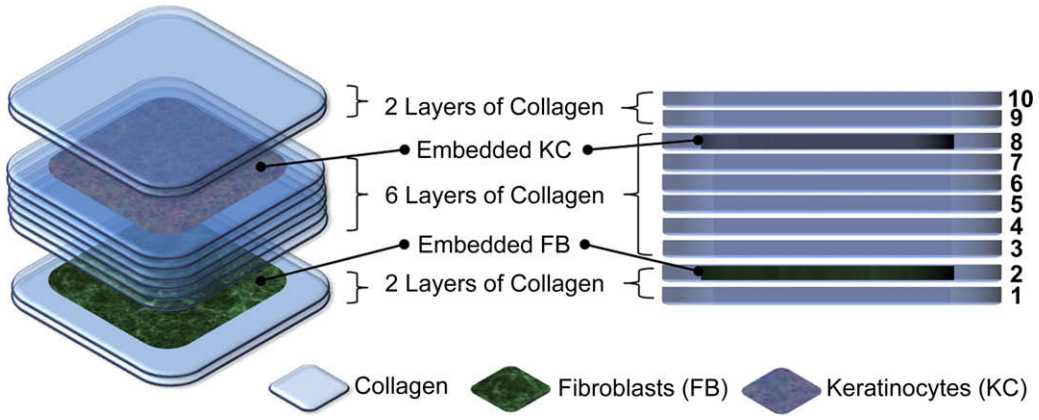

Fig. 3. Schematic of layer-by-layer printing of the multi-layered skin cells and collagen (left panel) including its side view (right panel). FB were printed in the 2nd collagen layer, and six layers of collagen were printed over the FB. KC were printed in the 8th layer of collagen and two layers of collagen were used to cover the KC layer.

resolution of 300 μm was selected for subsequent 3D printing experiments. A simple 2D 'plus' shaped FB pattern, consisting of 5-mm-long vertical and horizontal lines, was printed at the same printing resolution.

2.8. On-demand planar multi-layer cell–hydrogel printing

Using the method described to enable the construction of multi-layer cell–collagen composites, a total of 10 layers of collagen were sequentially printed on planar square in a 60 mm tissue culture dish (Fig. 3). FB and KC layers were located in the second and the eighth layer of collagen hydrogel (counted from the bottom layer), respectively. Five layers of collagen were sandwiched between the layers of FB and KC to demonstrate the ability to print spatially distinctive cell layers. Upon printing, the cell–collagen composites were cultured in 37 °C, 5% CO_2 in KC media. The medium was changed every other day.

2.9. A PDMS mold of 3D skin wound model

A PDMS mold, which simulates a shape of non-planar skin wound, was constructed to examine the ability to directly print multi-layered cell–collagen composites on a 3D surface. PDMS is biologically inert and provides excellent optical transparency for observing the printed cell–hydrogel composites on it. To construct the PDMS mold, an aluminum cast was prepared to imprint a negative mold having 3D contours (Fig. 4A) with a surface area of ~250 mm^2. The cast was then positioned in the middle of 60 mm tissue culture dish while a 10:1 mixture of PDMS prepolymer and curing agent (Sylgard 184 silicone elastomer kit; Dow Corning, Midland, MI) was degassed and poured onto the cast. This dish was allowed to cure for 24 h in a laminar hood. The wound model was kept in the tissue culture dish so that cell culture media could be added after cell–hydrogel printing.

For the direct cell printing on the non-planar PDMS wound model, the desired printing patterns were obtained from the CAD file of the model, and its spatial dimension and shape were used to plan the 3D printing patterns in multiple layers (a sequence of the printed planar layer for the model is shown in Fig. 4C). The distance between the nozzle and the target substrates was maintained at 5 mm. Another method of printing, although not used in this experiment, was to follow the contour of the non-linear surface while filling non-planar surface. Although the collagen precursor was dispensed onto the curved surface of the PDMS mold, the surface treated with $NaHCO_3$ retained the subsequent layers of printed morphology.

2.10. Live/dead staining for viability test of dispensed cells

A cell viability assay was performed on the printed cells 3 h after dispensing using a commercially available live/dead assay kit (Molecular Probes, MA). A group of unprinted cells were separately prepared as a control group. The samples were rinsed with DPBS and incubated for 40 min in a solution of 5 μL of calcein AM and 20 μL of ethidium homodimer-1 in 10 mL of DPBS (dead cells show red and live cells show green). Cellular fluorescence was observed in an inverted epifluorescent microscope (Olympus USA, Melville, NY) using FITC/RhoA band filters.

2.11. Immunohistochemistry (IHC) for immunostaining

β-Tublin (cytoskeleton, Cell Signaling Technology, Inc., Danvers, MA) and pan-keratin (keratin, Cell Signaling Technology, Inc., Danvers, MA) were used to label key cellular features of both FB and KC printed in the tissue culture dish. The main differentiating cell label was anticipated to be keratin as KC have an abundant source of keratin, while FB lack the presence of keratin. The printed multi-layered cell–collagen composites cultured for 4 days were rinsed in 1 × phosphate-buffered saline (PBS), fixed with 4% formaldehyde for 15 min, and rinsed three times in 1 × PBS for 5 min each. After incubating in the blocking solution (5% normal mouse serum and 5% normal rabbit serum prepared in PBS with Triton X-100) for 60 min at room temperature, printed cell–collagen composites were exposed to pan-keratin (C11) mouse monoclonal antibody and β-tubulin (9F3) rabbit monoclonal antibody diluted in 1 × PBS (tubulin = 1:200 in PBS; keratin = 1:200 in PBS) overnight at 4 °C. Consequently, fluorescence-labeled secondary antibodies were applied. The 3D architecture of stained samples was visualized using a Nikon C1 confocal system.

3. Results

3.1. Droplet size, cells per droplet, and viability assay of printed skin cells

The dispensed droplet volume of cell suspension was 8.1 ± 2.1 nL, when measured at 1 psi with a microvalve opening time of 450 μs. The volume of collagen precursor at given dispensing condition (2 psi with valve opening time of 600 μs) was 7.6 ± 2.7 nL. At 10^6 cells/mL, the number of cells contained in each droplet was measured to be 93 ± 13 cells/droplet for FB and 68 ± 13 cells/droplet for KC ($n = 36$). The number of cells contained in each droplet was several times larger than the theoretical calculation of 23 cells/droplet at the given cell suspension density (concentration of 1×10^6 cells/mL).

The morphology of the printed cells was monitored after day 1 of culture. There was no morphological difference observed for either printed FB or KC, when compared to manually plated cells. The viability of control FB was $96.6 \pm 3.9\%$ while printed FB showed the viability of $95.0 \pm 2.3\%$ ($n = 30$). The viability of control KC was $83.9 \pm 7.1\%$ and that of printed KC was $85.5 \pm 5.7\%$ ($n = 30$). There was no significant difference in viability of printed FB and KC compared to each control group ($p > 0.05$; t-test two-tailed), suggesting that the cell dispensing method did not affect the cell viability.

3.2. Testing of different printing resolutions and patterning in 2D

The FBs printed at different spatial resolutions were observed under a bright-field microscope. The FBs printed in low printing resolution (700 and 900 μm; data not shown) did not reach sufficient cell growth in 7 days. The attempt to print the cells at a high (200 μm) resolution resulted in failure of proper encapsulation in collagen bed due to excessive amounts of media compared to the surface area of the printed collagen material. Day 1 culture images of Fig. 5A–C showed the cell density difference among the three

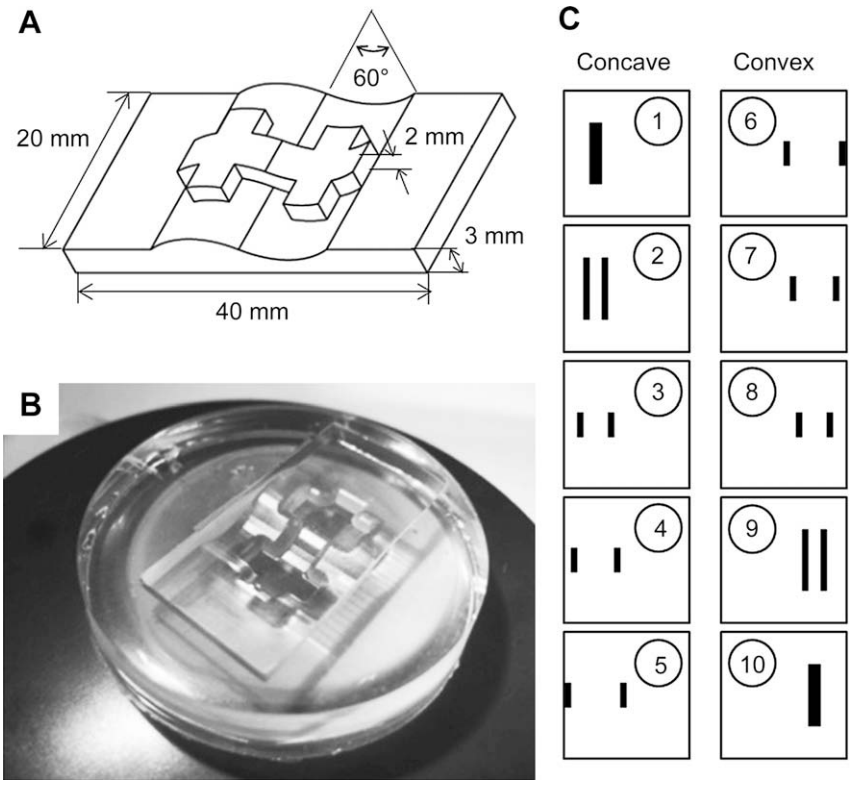

Fig. 4. Fabrication of a PDMS mold of 3D skin wound model. (A) The negative mold with 3D contour for a PDMS mold of 3D skin wound model. The aluminum cast was prepared to imprint this negative mold and used to construct a PDMS mold. (B) Prepared PDMS mold of 3D skin wound model. Multiple layers of collagen and skin cells were printed onto the 3D mold surface of the wound model. (C) The image sequence used for printing of collagen and cells.

groups with different printing resolutions (300, 400, and 500 μm inter-dispensing distance). The sparsity of the cells created by adjusting the printing resolution was apparent from the pictures that were taken on Day 1. After 8 days of culture, printed FB with 300 μm resolution showed the highest cell density when compared to the other groups. A similar cell density was shown between printed FB in 400 μm resolution and those in 500 μm resolution. In the culture of FB in collagen hydrogel, textured pattern (co-aligned cell distributions) of FB growth was observed, and the FB printed in higher resolution (300 μm) showed the texture pattern first (Fig. 5D). Fig. 5G shows the 2D printing of a plus shape FB pattern imaged on Day 1. After 7 days of culture, the pattern could no longer be identified due to excessive cell proliferation (data not shown).

3.3. On-demand planar multi-layered printing of FB and KC

Fig. 6A–C shows confocal microscope images of printed multi-layered FB and KC at Day 4 of culture after immunostaining. Imaging software (Nikon EX-C1) was used to alternate the presence of each fluorescent dye in the image (Fig. 6A with volume rendered sample). Nuclei are labeled in blue while keratin and β-tublin are labeled in green and red, respectively. Fig. 6B shows the keratin-containing KC layer with spherical morphology. Fig. 6C (β-tublin labeling) illustrates that both bottom and upper cell layers contain β-tublin. FB layer, approximately 100 μm below the surface of the culture media, shows extensive tree-like morphology which is common in a 3D culture environment [31]. The clear distinctive

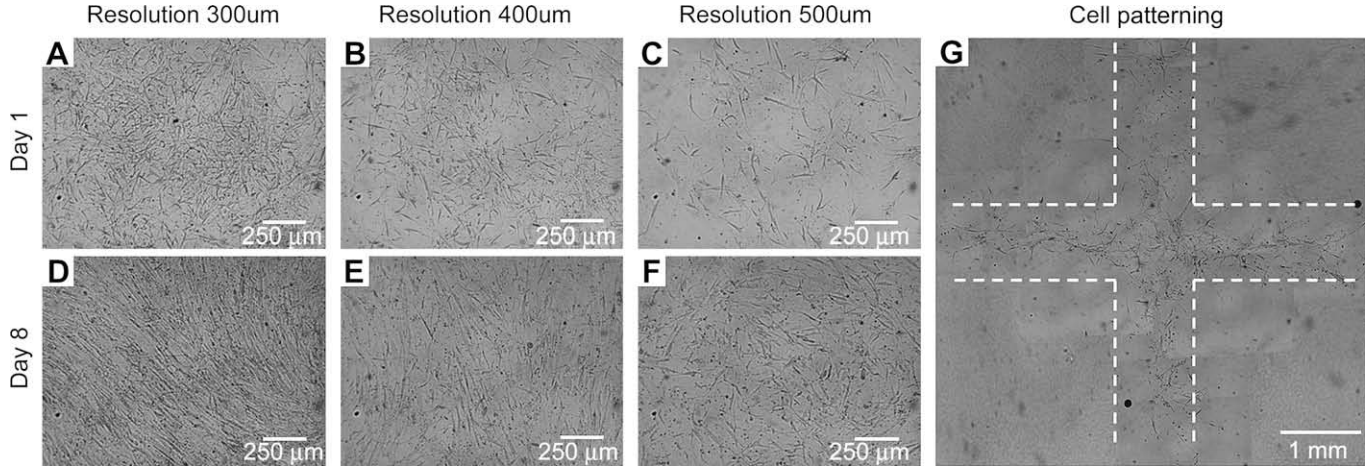

Fig. 5. Culture images at Day 1 (A–C) and Day 8 (D–F) of FB printed in 300 μm, 400 μm, and 500 μm resolution. Inter-dispensing distance of 300 μm showed confluent cell density on Day 8. The right panel (G) shows the on-demand 2D printing of a plus shape, with dotted lines indicating the printing profile.

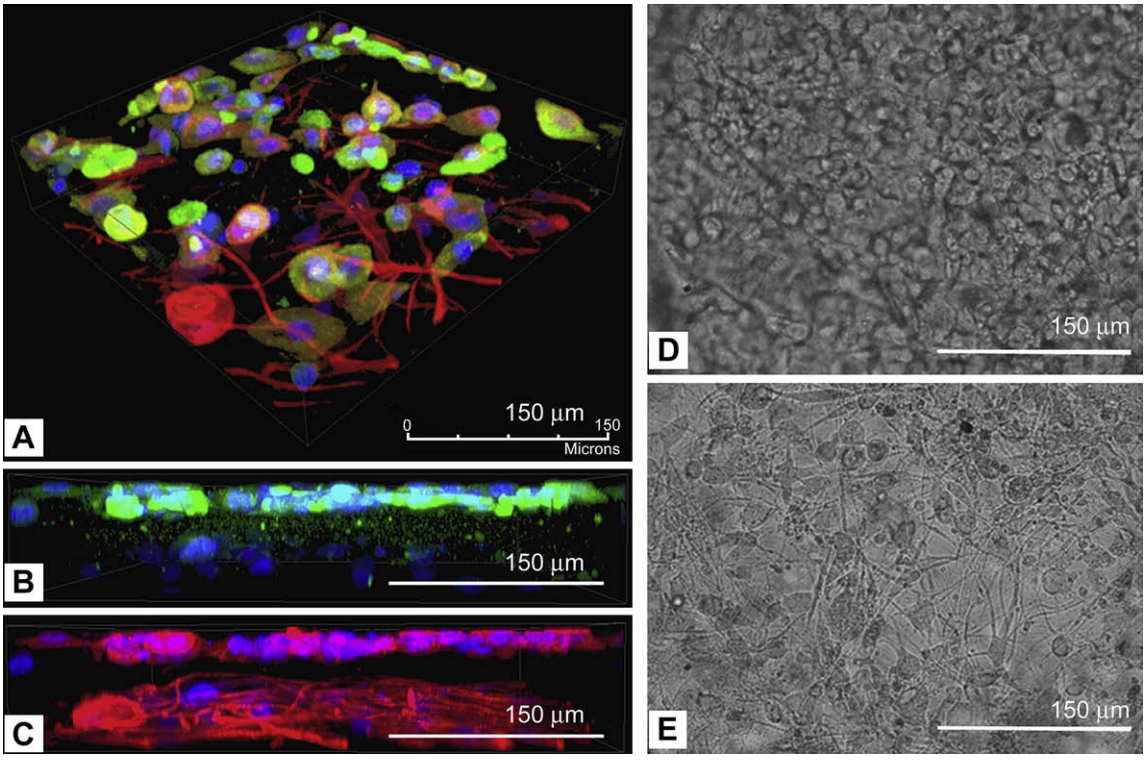

Fig. 6. Cell images after multi-layered printing of FB and KC on the tissue culture dish. (A) Volume rendered immunofluorescent images of multi-layered printing of KC and FB and its projection of (B) keratin-containing KC layer and (C) β-tublin-containing KC and FB. The interlayer distance of approximately 75 μm was observed. Bright-field images on (D) KC layer and (E) FB layer also confirmed the IHC findings.

layers of FB and KC were visible under the projection images in Fig. 6B and C. An interlayer distance of approximately 75 μm was observed, suggesting that each collagen layer occupied about 15 μm. Fig. 6D and E is the bright-field images of KC and FB layers after 3 days in culture, respectively.

3.4. On-demand non-planar multi-layer printing and culture of FB and KC for 3D skin wound model

Fig. 7 shows the results obtained from multi-layered printing of FB and KC on a non-planar PDMS surface mimicking a 3D skin wound model. FB and KC layers were embedded in the 2nd and the 8th layers of collagen scaffold from bottom, respectively. Fig. 7A and B is the images of printed cell–collagen composite on the PDMS mold. The surface of cell–collagen was wrinkled due to the cell suspension printing over collagen layers and the cell attachments in collagen scaffold. The distance of FB and KC layers at the concave area was approximately 100 μm; however the distance found in the convex area was reduced to approximately 60 μm. Fig. 7C and D shows bright-field images of KC and FB layers located in a same field-of-view (pictured in Day 1). Both bright-field images of KC and FB layers show varying depth of focus from upper left area to lower right area, which show the 3D contour of the PDMS mold surface.

4. Discussion

We developed and implemented a high-precision, multi-channel robotic printer and software environment to create 3D collagen hydrogel structure mimicking stratified skin. Hydrogel-based scaffolds, compared to the solid-state scaffold material, offer a biodegradable structure with sufficient gas-permeability to transfer oxygen and other nutrients in soluble forms [32]. Hydrogels have natural porosity as compared to other solid scaffolds with porosity and therefore have superior biocompatibility with the existing tissue environment and cell viability compared to the solid ones [33]. Hydrogels also offer unique 3D ECM scaffolds for proper growth and differentiation of chondrocytes or hepatocytes [34].

For the construction of a hydrogel scaffold using the 3D FF process, we introduced a new method to crosslink the printed hydrogel precursors. Instead of dipping the printed materials into the solution containing the crosslinker, the nebulized mists of crosslinking agent were coated on the surface before and after the printing of each layer of hydrogel composites. Crosslinking agents may optionally be prepared as a solid material in the target substrates; however, rather slow diffusion-based crosslinking would prohibit the efficient construction of the multi-layered hydrogel structure. We demonstrated that our method successfully printed multi-layer cell–hydrogel construct. The proposed method can be applied to virtually all chemically (including pH sensitive) crosslinkable hydrogels as long as either the hydrogel precursor or the crosslinking materials can be used to coat the printed hydrogel surface.

Another advantage of the proposed method is that hydrogel–cell composites can be built on non-planar surfaces since the crosslinking agents can be nebulized and coat the surface. Existing hydrogel 3D FF techniques [26,27,29] rely on dispensing of one of the hydrogel precursor/crosslinking materials to the "bed" of liquid crosslinker/hydrogel precursor. Therefore, direct construction of the hydrogel on non-planar surface would require a separate container that houses the materials around the surface parameter. As demonstrated by the results obtained from the PDMS wound model as shown in Fig. 7C, a printed tissue composite can be directly built on an irregular, non-planar surface without the needs for having containers for crosslinking material.

In addition to having the ability to construct 3D hydrogel structures via direct FF technique, another crucial technical feature

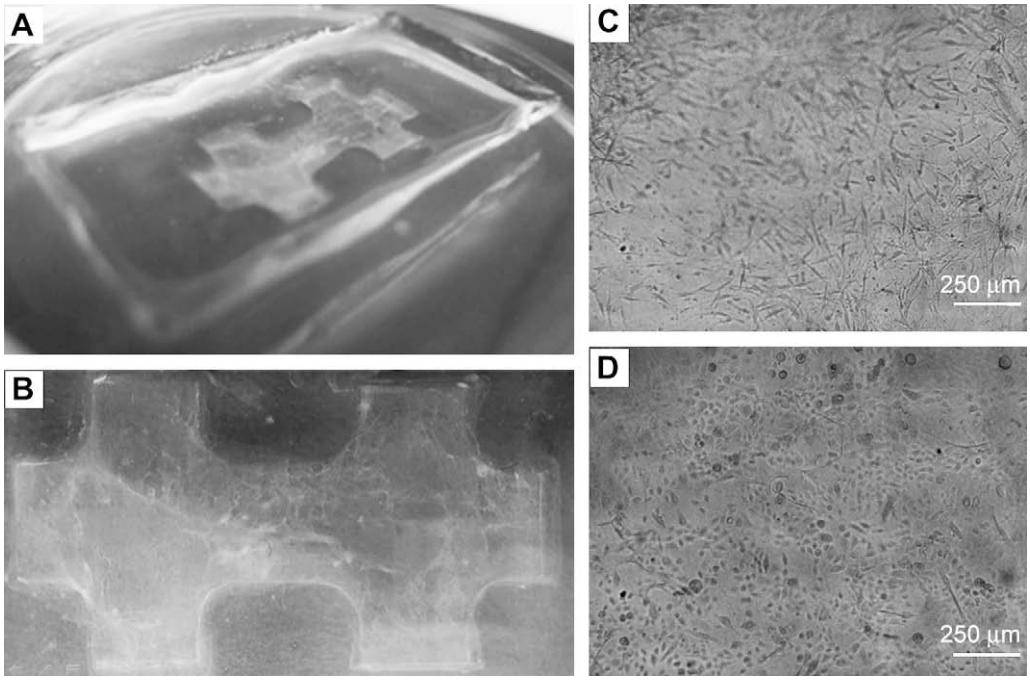

Fig. 7. Cell images after multi-layered printing of FB and KC on the PDMS mold. (A) An image (obtained in Day 1 of culture) after the multi-layered printing of FB and KC on PDMS mold of 3D skin wound model. (B) Top view of printed multi-layer cell–collagen composite on the PDMS mold of the wound model. The bright-field images of (C) KC and (D) FB layers obtained from the same field-of-view.

required for the generation of cell–hydrogel composites was to dispense the cells and hydrogel precursor precisely on the target without direct contact with the target surface. Several non-contact direct cell dispensing methods have been introduced. These include cell dispensing using ink-jet printing [23,29,35–38] or laser-printing technology [39–41]. Ink-jet cell printing uses a modified commercial version of bubble jet (heat-induced instant bubble formation and concurrent displacement of surrounding liquid) or piezoelectric methods to dispense cells in suspension. The laser-printing technique is based on the instant focus of a high-energy laser to the focal spot above a cell-laden substrate and subsequent dispensing of the cells under the 'evaporated' focal point. These approaches, however, may damage cells due to excessive pressure and temperature during droplet generation, high shear stresses at the nozzle, or nozzle clogging [38,42]. Moreover, the laser-printing method cannot reach high-throughput rates with continuous dispensing of cells due to the need for "cell-laden strips" [41,43].

We used electromechanical microvalves with a relatively large nozzle diameter of 150 μm operating under low pneumatic pressure to provide flexibility in experiment and permitting non-contact dispensing of droplet. Another advantage of using the microvalves was that the droplet volume can be adjusted by controlling the pressure to the fluidic pathway and valve opening time, allowing for the dispensing of liquids with different viscosities. High cell viabilities for FB and KC were acquired at operating pressure of 1.0–1.2 psi. There was no significant difference in cell viabilities between printed cells and manually plated cells as demonstrated in the viability assay. Although long-term monitoring of the printed cell composites was not performed, contraction of the collagen containing cell matrix was observed toward the end of the two weeks culture period. This contraction, as anticipated via interconnected collagen fibril [44,45], can be relieved by the addition of supporting materials such as glycosaminoglycan or decorin [46].

In terms of the concentration of the cells in suspension, our results indicate that an excessive number of FB ($>3.0 \times 10^6$ cells/mL) clogged the dispenser while low cell density ($<10^5$ cells/mL) did not promote proper cell growth. This suggests that a degree of optimization is needed in regard to the properties of each cell line such as cell size, shape, and tendency to aggregate each other. In addition, we have observed that number of cells in the droplet was four times (in the case of FB) and three times (in the case of KC) more than the theoretical calculation based on the prepared cell density. We conjecture that cell sedimentation and aggregation occurring between the time of cell preparation and actual printing procedure might have contributed to the increased number of cells in each droplet. Further design improvement of the dispensing pathway is being made to maintain the original cell density via more thorough mixing/agitation of the cell-containing syringes.

For cell concentrations of FB and KC at 1.0×10^6 cells/mL, 2D (Fig. 5G) and 3D cell patterning and culture were achieved with printing resolution of 300 μm. With higher printing resolutions, excessive culture medium was dispensed on collagen padding layer, while with lower printing resolutions, low level of proliferation of printed cells was observed due to low cell density. This indicates the necessity to optimize the printing density in 2D plane prior to the construction of 3D tissue composite. Regarding the height of the constructed skin tissue composite, we introduced acellular hydrogel layers between the layers of FB and KC to form a distinctive cell layers (Fig. 6A). The gap between two layers, after the culture period, was approximately 75 μm. It suggests that relative gap between the dispensed cell layers can be adjusted by altering the number of collagen layers between.

An FB layer printed in the 2nd layer of collagen successfully proliferated, indicating that 8 printed layers of collagen permitted the diffusion of oxygen and other nutrients into the cell layer via passive diffusion across the hydrogel block [47]. As the resolution achieved in this work is in the order of 700 μm to 1 mm, this may limit the application for tissues thicker than 100 μm, which is beyond the passive diffusion limits in biological tissue (in the order of 100 and 200 μm [48]). Therefore, improvements to the dispenser and printing mechanism accommodating higher printing

resolution are needed. In order to increase the thickness of viable cell–collagen composites, fluidic channels should be introduced inside the hydrogel to provide adequate perfusion. Based on our FF technique, sacrificial fluidic channels can be printed (for example, using temperature-sensitive gelatin [18]) in the middle of the collagen scaffold, and later be removed to create on-demand hydrogel channels. This may offer expedited construction of the hydrogel channel via multi-layered soft-lithographic approaches [17–19]. Further investigation is warranted to demonstrate such ability.

We also tested the feasibility of using the printer to create the multi-layered skin cell–hydrogel composites directly printed on a PDMS mold with non-planar contour. Although there was a presence of inhomogeneous distribution in depth, distinct layers of FB and KC were evident with normal proliferation after printing. These results suggest that direct printing of cells and hydrogel composites of biological and non-biological origin may substitute the damaged skin layers. A potential advantage of the approach over the conventional skin graft is that the wound-specific skin layers can be printed directly in an on-demand fashion with the help of computer-aided planning. This would provide the opportunity to optimize/predict the quantity of the skin cells needed, most likely the cultured autologous cells, for the wound site graft. Animal *in vivo* testing on skin wound healing is needed to confirm this hypothesis.

In addition to its potential application for tissue engineered skin regeneration, we anticipate the developed technique to be used to study various aspects of wound healing, skin diseases, and connective tissue regeneration [4,14,49]. For example, by printing and culturing different cell lines like melanocytes, melanomas, or epithelial cells with FB and KC in multi-layered collagen scaffold, the current method can be used to construct an *in vitro* skin disease model with cells of different phenotypes or disease progress stage, and may potentially serve as a large-scale high-throughput platform for drug testing and development. Incorporation of more realistic organotypic culture method, which involves air–liquid interface model [16] will be needed to generate skin-like epidermal layer.

5. Conclusions

In this study, we developed and implemented a novel 3D bioprinter using electromechanical microvalve with high cell viability. On-demand 3D multi-layered printing and culture of human FB and KC were demonstrated utilizing collagen hydrogel as a scaffold material. Using computer-controlled dispensing of skin cells and hydrogels layer-by-layer, the feasibility of skin regeneration and wound-specific tissue engineered skin product was also demonstrated via *in vitro* wound model. To our knowledge, this is the first study of printing both FB and KC in a single experiment with the formation of dermal/epidermal-like distinctive layers in a 3D hydrogel scaffold. The technique can be applied to a wide range of applications from drug screening to creating tissue engineered products.

Acknowledgements

We gratefully acknowledge the unconditional assistance in cell imaging by Dr. Randy Wetzel and the Cytometry Team at Cell Signaling Technology, Inc. in Danvers, MA. We also thank the Chung Moon Soul Center for BioInformation and BioElectronics, KAIST.

Appendix

Figures with essential colour discrimination. Certain figures in this article, in particular parts of Figs. 1 and 6, are difficult to interpret in black and white. The full colour images can be found in the on-line version, at doi:10.1016/j.biomaterials.2008.12.009.

References

[1] Ben-Bassat H, Chaouat M, Segal N, Zumai E, Wexler MR, Eldad A. How long can cryopreserved skin be stored to maintain adequate graft performance? Burns 2001;27(5):425–31.
[2] Atiyeh BS, Hayek SN, Gunn SW. New technologies for burn wound closure and healing–review of the literature. Burns 2005;31(8):944–56.
[3] Wood FM, Kolybaba ML, Allen P. The use of cultured epithelial autograft in the treatment of major burn injuries: a critical review of the literature. Burns 2006;32(4):395–401.
[4] MacNeil S. Progress and opportunities for tissue-engineered skin. Nature 2007;445(7130):874–80.
[5] Burke JF, Yannas IV, Quinby Jr WC, Bondoc CC, Jung WK. Successful use of a physiologically acceptable artificial skin in the treatment of extensive burn injury. Ann Surg 1981;194(4):413–28.
[6] Cuono C, Langdon R, McGuire J. Use of cultured epidermal autografts and dermal allografts as skin replacement after burn injury. Lancet 1986;1(8490):1123–4.
[7] Stern R, McPherson M, Longaker MT. Histologic study of artificial skin used in the treatment of full-thickness thermal injury. J Burn Care Rehabil 1990;11(1):7–13.
[8] Boyce ST, Goretsky MJ, Greenhalgh DG, Kagan RJ, Rieman MT, Warden GD. Comparative assessment of cultured skin substitutes and native skin autograft for treatment of full-thickness burns. Ann Surg 1995;222(6):743–52.
[9] Boyce ST, Kagan RJ, Yakuboff KP, Meyer NA, Rieman MT, Greenhalgh DG, et al. Cultured skin substitutes reduce donor skin harvesting for closure of excised, full-thickness burns. Ann Surg 2002;235(2):269–79.
[10] Supp DM, Boyce ST. Engineered skin substitutes: practices and potentials. Clin Dermatol 2005;23(4):403–12.
[11] Ralston DR, Layton C, Dalley AJ, Boyce SG, Freedlander E, Mac Neil S. The requirement for basement membrane antigens in the production of human epidermal/dermal composites in vitro. Br J Dermatol 1999;140(4):605–15.
[12] Sahota PS, Burn JL, Heaton M, Freedlander E, Suvarna SK, Brown NJ, et al. Development of a reconstructed human skin model for angiogenesis. Wound Repair Regen 2003;11(4):275–84.
[13] Sun T, Mai S, Norton D, Haycock JW, Ryan AJ, MacNeil S. Self-organization of skin cells in three-dimensional electrospun polystyrene scaffolds. Tissue Eng 2005;11(7-8):1023–33.
[14] Barker CL, McHale MT, Gillies AK, Waller J, Pearce DM, Osborne J, et al. The development and characterization of an in vitro model of psoriasis. J Invest Dermatol 2004;123(5):892–901.
[15] Eves P, Katerinaki E, Simpson C, Layton C, Dawson R, Evans G, et al. Melanoma invasion in reconstructed human skin is influenced by skin cells–investigation of the role of proteolytic enzymes. Clin Exp Metastasis 2003;20(8):685–700.
[16] Gangatirkar P, Paquet-Fifield S, Li A, Rossi R, Kaur P. Establishment of 3D organotypic cultures using human neonatal epidermal cells. Nat Protoc 2007;2(1):178–86.
[17] Bettinger CJ, Weinberg EJ, Kulig KM, Vacanti JP, Wang Y, Borenstein JT, et al. Three-dimensional microfluidic tissue-engineering scaffolds using a flexible biodegradable polymer. Adv Mater 2006;18(2):165–9.
[18] Golden AP, Tien J. Fabrication of microfluidic hydrogels using molded gelatin as a sacrificial element. Lab Chip 2007;7(6):720–5.
[19] King KR, Wang CCJ, Kaazempur-Mofrad MR, Vacanti JP, Borenstein JT. Biodegradable microfluidics. Adv Mater 2004;16(22):2007–12.
[20] Boland T, Mironov V, Gutowska A, Roth EA, Markwald RR. Cell and organ printing 2: fusion of cell aggregates in three-dimensional gels. Anat Rec A Discov Mol Cell Evol Biol 2003;272(2):497–502.
[21] Sachlos E, Czernuszka JT. Making tissue engineering scaffolds work. Review: the application of solid freeform fabrication technology to the production of tissue engineering scaffolds. Eur Cell Mater 2003;5:29–39.
[22] Burg KJ, Boland T. Minimally invasive tissue engineering composites and cell printing. IEEE Eng Med Biol Mag 2003:84–91.
[23] Mironov V, Boland T, Trusk T, Forgacs G, Markwald R. Organ printing: computer-aided jet-based 3D tissue engineering. Trends Biotechnol 2003;21(4):157–61.
[24] Mironov V, Drake C, Wen X. Research project: Charleston bioengineered kidney project. Biotechnol J 2006;1(9):903–5.
[25] Sun W, Darling A, Starly B, Nam J. Computer-aided tissue engineering: overview, scope and challenges. Biotechnol Appl Biochem 2004;39(Pt 1):29–47.
[26] Boland T, Tao X, Damon BJ, Manley B, Kesari P, Jalota S, et al. Drop-on-demand printing of cells and materials for designer tissue constructs. Mater Sci Eng C 2007;27(3):372–6.
[27] Chang R, Nam J, Sun W. Direct cell writing of 3D microorgan for In vitro pharmacokinetic model. Tissue Eng Part C Methods 2008;14(2):157–66.
[28] Hill DL, Batchelor PG, Holden M, Hawkes DJ. Medical image registration. Phys Med Biol 2001;46(3):R1–45.
[29] Boland T, Xu T, Damon B, Cui X. Application of inkjet printing to tissue engineering. Biotechnol J 2006;1(9):910–7.
[30] Chang R, Nam J, Sun W. Effects of dispensing pressure and nozzle diameter on cell survival from solid freeform fabrication-based direct cell writing. Tissue Eng Part A 2008;14(1):41–8.

[31] Toriseva MJ, Ala-aho R, Karvinen J, Baker AH, Marjomäki VS, Heino J, et al. Collagenase-3 (MMP-13) enhances remodeling of three-dimensional collagen and promotes survival of human skin fibroblasts. J Invest Dermatol 2007;127(1):49–59.
[32] Yeh J, Ling Y, Karp JM, Gantz J, Chandawarkar A, Eng G, et al. Micromolding of shape-controlled, harvestable cell-laden hydrogels. Biomaterials 2006; 27(31):5391–8.
[33] Drury JL, Mooney DJ. Hydrogels for tissue engineering: scaffold design variables and applications. Biomaterials 2003;24(24):4337–51.
[34] Griffith LG, Swartz MA. Capturing complex 3D tissue physiology in vitro. Nat Rev Mol Cell Biol 2006;7(3):211–24.
[35] Roth EA, Xu T, Das M, Gregory C, Hickman JJ, Boland T. Inkjet printing for high-throughput cell patterning. Biomaterials 2004;25(17):3707–15.
[36] Wilson Jr WC, Boland T. Cell and organ printing 1: protein and cell printers. Anat Rec A Discov Mol Cell Evol Biol 2003;272(2):491–6.
[37] Xu T, Petridou S, Lee EH, Roth EA, Vyavahare NR, Hickman JJ, et al. Construction of high-density bacterial colony arrays and patterns by the ink-jet method. Biotechnol Bioeng 2004;85(1):29–33.
[38] Xu T, Jin J, Gregory C, Hickman JJ, Boland T. Inkjet printing of viable mammalian cells. Biomaterials 2005;26(1):93–9.
[39] Barron JA, Wu P, Ladouceur HD, Ringeisen BR. Biological laser printing: a novel technique for creating heterogeneous 3-dimensional cell patterns. Biomed Microdevices 2004;6(2):139–47.
[40] Ringeisen BR, Chrisey DB, Pique AP, Young HD, Modi R, Bucaro M, et al. Generation of mesoscopic patterns of viable Escherichia coli by ambient laser transfer. Biomaterials 2002;23(1):161–6.
[41] Ringeisen BR, Kim H, Barron JA, Krizman DB, Chrisey DB, Jackman S, et al. Laser printing of pluripotent embryonal carcinoma cells. Tissue Eng 2004; 10(3-4):483–91.
[42] Xu T, Gregory CA, Molnar P, Cui X, Jalota S, Bhaduri SB, et al. Viability and electrophysiology of neural cell structures generated by the inkjet printing method. Biomaterials 2006;27(19):3580–8.
[43] Chen CY, Barron JA, Ringeisen BR. Cell patterning without chemical surface modification: Cell-cell interactions between printed bovine aortic endothelial cells (BAEC) on a homogeneous cell-adherent hydrogel. Appl Surf Sci 2006;252(24):8641–5.
[44] Bell E, Ehrlich HP, Buttle DJ, Nakatsuji T. Living tissue formed in vitro and accepted as skin-equivalent tissue of full thickness. Science 1981;211(4486):1052–4.
[45] Bittner K, Liszio C, Blumberg P, Schönherr ES, Kresse H. Modulation of collagen gel contraction by decorin. Biochem J 1996;314(Pt 1):159–66.
[46] Gentleman E, Nauman EA, Dee KC, Livesay GA. Short collagen fibers provide control of contraction and permeability in fibroblast-seeded collagen gels. Tissue Eng 2004;10(3–4):421–7.
[47] Ling Y, Rubin J, Deng Y, Huang C, Demirci U, Karp JM, et al. A cell-laden microfluidic hydrogel. Lab Chip 2007;7(6):756–62.
[48] Parker KK, Ingber DE. Extracellular matrix, mechanotransduction and structural hierarchies in heart tissue engineering. Philos Trans R Soc Lond B Biol Sci 2007;362(1484):1267–79.
[49] Hedley SJ, Layton C, Heaton M, Chakrabarty KH, Dawson RA, Gawkrodger DJ, et al. Fibroblasts play a regulatory role in the control of pigmentation in reconstructed human skin from skin types I and II. Pigment Cell Res 2002;15(1):49–56.